Chemical Engineering Journal 487 (2024) 150659

Contents lists available at ScienceDirect

Chemical Engineering Journal

journal homepage: www.elsevier.com/locate/cej

Intercalation of small molecules in the selective layer of polyamide nanofiltration membranes facilitates the separation of Mg^{2+}/Li^{+}

Junwei Li [a,1], Long Fang [b,1], Daliang Xu [c], Xi Zhang [d], Lei Jiang [a], Qingjuan Zhu [e], Qin Chen [a], Pengrui Jin [a], Alexander Volodine [f], Raf Dewil [d], Xiahui Gui [b,*], Qieyuan Gao [a,*], Bart Van der Bruggen [a,*]

[a] Department of Chemical Engineering, KU Leuven, Celestijnenlaan 200F, B-3001 Leuven, Belgium
[b] State Key Laboratory of Coking Coal Resources Green Exploitation, China University of Mining and Technology, Xuzhou, 221116, Jiangsu, China
[c] State Key Laboratory of Urban Water Resource and Environment, School of Environment, Harbin Institute of Technology, Harbin, 150090, China
[d] Department of Chemical Engineering, KU Leuven, Process and Environmental Technology Lab, J. De Nayerlaan 5, 2860 Sint-Katelijne-Waver, Belgium
[e] Laboratory of Molecular Cell Biology, Department of Biology, Institute of Botany and Microbiology, KU Leuven, 3001 Leuven, Belgium
[f] Department of Physics and Astronomy, KU Leuven, Celestijnenlaan 200D, B-3001 Leuven, Belgium

ARTICLE INFO

Keywords:
Nanofiltration
Lithium separation
Positive charge
Polyamide membrane
Aminomalononitrile (AMN)

ABSTRACT

In addressing lithium supply shortages driven by increased energy demand, nanofiltration membrane technology is crucial for recovering lithium from salt lake brines. Overcoming the challenge of achieving high selectivity for Li^{+} and water permeability in polymer nanofiltration membranes, this study proposes a simple approach using Aminomalononitrile (AMN) intercalation to modify polyamide layers. Density functional theory simulations predict AMN's superior selectivity and enhanced hydrophilicity. Stable intercalation of AMN between polyethyleneimine (PEI) molecules is demonstrated, synergistically enhancing water permeability and Li^{+} selectivity. The resulting PEI/AMN-TMC membrane exhibits exceptional Li^{+} selectivity and improved water permeability (13.1 $L{\cdot}m^{-2}{\cdot}h^{-1}{\cdot}bar^{-1}$), 2.9 times higher than traditional PEI-TMC membranes. Stable performance for over seven days, along with anti-scaling and anti-bacterial properties, underscores its practicality. This investigation sheds light on membrane structure regulation through small-molecule intercalation, offering insights into precise adjustments for enhanced water permeability and ion selectivity.

1. Introduction

With the successful development of Li-ion batteries in portable electronics and electric vehicles, there has been a significant surge in demand for lithium [1,2]. Salt lake brines characterized by a low magnesium-lithium ratio contribute to approximately 60 % of lithium compounds [3]. However, the retrieval of lithium from salt lake brines with a high Mg^{2+}/Li^{+} ratio has garnered significant attention owing to the substantial demand for lithium resources (e.g., electro-driven [4,5], solvent extraction [6,7], precipitation [8], adsorption [9]). Benefiting from the size sieving and Gibbs-Donnan effect, nanofiltration intends to be an environmentally friendly and easy-to-operate lithium recovery technology [10]. In nanofiltration membranes, the Gibbs-Donnan effect manifests as an additional mechanism alongside the sieving effect. As solute concentration rises, the membrane can not only reject solutes larger than its pore size (sieving effect) but also repel ions in the solution that bear the same electrical charge as the membrane surface. This phenomenon is particularly pronounced in positively charged membranes, leading to heightened rejection of positively charged molecules. Nowadays, positively charged polyamide nanofiltration membranes and their derivatives fabricated by interfacial polymerization of polyethyleneimine (PEI) and 1,3,5-benzenetricarbonyl trichloride (TMC) have been widely used in the removal of heavy metal cations from solutions, and the separation of divalent ions [11,12]. The standard PEI-TMC membrane exhibits specific selectivity for separating Mg^{2+} and Li^{+}. However, its practical performance is constrained by the relatively low water permeance (~5 $L{\cdot}m^{-2}{\cdot}h^{-1}{\cdot}bar^{-1}$) resulting from the dense polyamide layer structure that is densely packed with long-chain PEI molecules [13].

To enhance the water permeance of PEI-TMC membranes and

* Corresponding authors.
E-mail addresses: guixiahui1985@163.com (X. Gui), qieyuan.gao@kuleuven.be (Q. Gao), bart.vanderbruggen@kuleuven.be (B. Van der Bruggen).
[1] Junwei Li and Long Fang contributed equally to this work.

https://doi.org/10.1016/j.cej.2024.150659
Received 4 December 2023; Received in revised form 15 March 2024; Accepted 23 March 2024
Available online 26 March 2024
1385-8947/© 2024 Elsevier B.V. All rights reserved.

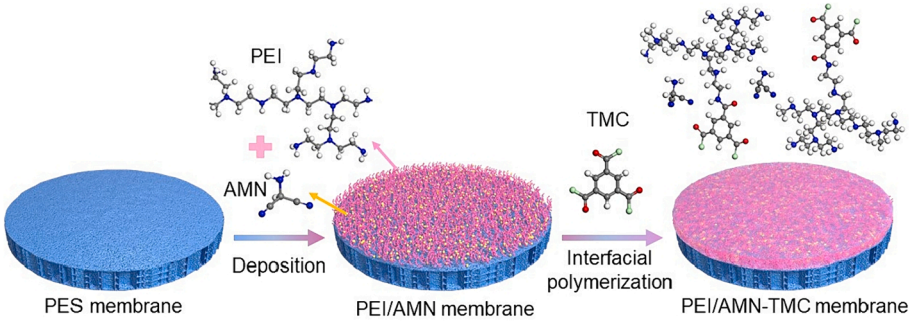

Fig. 1. Schematic illustration for the fabrication of PEI/AMN-TMC. Gray, blue, white, red, and green balls represent carbon, nitrogen, hydrogen, oxygen, and chlorine, respectively. (For interpretation of the references to colour in this figure legend, the reader is referred to the web version of this article.)

achieve a more rapid mass transfer by regulating the structure of the selective layer, nanomaterials such as quantum dots [9], graphene oxide [14], and carbon nitride [15] have been employed as additives. However, the practical utility of these materials is impeded by their high cost and complex synthesis process. Similarly, surface modification has shown promise in improving the permeance of polyamide membranes. Nonetheless, the intricate fabrication process and stringent conditions, including precise pH adjustment of the solution, impose limitations on its scalability for large-scale applications [16–18]. Positively charged modified polyamide membranes that have undergone extensive study continue to present a promising alternative. In the realm of electrochemistry for energy storage, heteroatom-doped carbon materials are frequently employed to increase the spacing between carbon layers, facilitating the rapid transport of metal ions. This approach has been widely adopted and verified in the development of carbon-based battery anode materials [19–23]. Taking inspiration from this concept, small molecules can be incorporated into the conventional PEI-TMC polyamide layer to increase the spacing between PEI chains, thus enhancing water permeability to address the issue of low permeability in the PEI-TMC polyamide layer. Aminomalononitrile (AMN) is a biochemically derived small molecule with an amino group, and its antibacterial attributes have been broadly substantiated and utilized [24,25]. Moreover, the -C≡N functional group of AMN endows it with stable chemical properties, suggesting that it can act as an intercalation molecule to expand the space between the stacked PEI long-chain molecules. The incorporation of a small molecule like AMN can provide PEI-TMC, the commonly used selective layer in Li recovery, with a specific scaffold structure. This can significantly ameliorate the common permeability issue arising from an overly dense polyamide layer. Furthermore, the presence of $–NH_2$ in AMN augments the positive charge of the selective layer, facilitating the exclusion of divalent ions to counterbalance the reduced rejection resulting from improved permeability. This has potential to break the permeation-rejection "trade-off" widespread in nanofiltration.

Here, a straightforward approach involving small-molecule intercalation was employed to incorporate AMN molecules between the long-chain molecules of PEI. This intercalation strategy was implemented to effectively expand the space between the PEI long-chain molecules, in view of an enhanced water permeance. Simultaneously, the $–NH_2$ group present in the AMN molecule can be protonated to $–NH_3^+$ in aqueous solution, which helps to enhance the positive charge of the polyamide membrane, thereby enhancing the repulsion of Mg^{2+}. Therefore, this strategy can elevate the positive charge of the PEI-TMC membrane to reinforce the Donnan effect and make the membrane structure looser to enhance the water permeance. Furthermore, the density functional theory (DFT) method was employed to predict and investigate the affinity of AMN and PEI molecules for water, as well as their repulsion for Li^+ and Mg^{2+}. DFT analysis confirmed that AMN could be effectively embedded between PEI long-chain molecules, leading to a significant increase in the spacing between the PEI chains. Such structural modification could significantly improve the water permeability of the PEI/AMN-TMC membrane. Consequently, the objective for PEI/AMN-TMC membranes presented here is to achieve enhanced water permeability, improved selectivity for Li^+ over Mg^{2+}, reliable long-term stability, excellent anti-fouling properties, and satisfactory antibacterial performance.

2. Materials and methods

2.1. Materials and chemicals

Ultrafiltration (UF) membrane casting solutions were prepared using polyethersulfone (PES) and dimethyl sulfoxide (DMSO, 99.5 %) obtained from BASF (Germany). n-Hexane (99 %) was supplied by VWR International BVBA, located in Leuven, Belgium. Sigma-Aldrich provided polyethyleneimine (PEI), trimesoyl chloride (TMC), lithium chloride (LiCl, 99 %), sodium chloride (NaCl, 99 %), sodium sulfate (Na_2SO_4, 99 %), magnesium chloride ($MgCl_2$, 98 %), magnesium sulfate ($MgSO_4$, 99 %), and aminomalononitrile (AMN). For the aqueous phase in the membrane preparation, a solvent of 100 mM phosphate-buffered saline (PBS) was employed, following the chemical selection outlined in the previous study conducted by our previous research [25].

2.2. Fabrication of AMN/PEI-TMC membranes

PES substrates were manufactured as a support layer via a traditional phase inversion method. The PES polymer (16 wt%) was dissolved in DMSO (84 wt%). Then, use a spatula to scrape the casting solution onto the non-woven fabric on the glass plate. Subsequently, the non-woven fabric was placed in deionized water (DI) and left for 30 min to ensure that the phase inversion reaction was fully carried out. The resulting membrane was then rinsed thoroughly with DI. A traditional interfacial polymerization (IP) reaction was applied to develop the active layer. The aqueous solution containing 0.0–0.7 wt% PEI and 0.0–0.9 wt% AMN was dissolved in the PBS buffer (10 ml) in a particular proportion on the membrane and was kept in contact with the membrane for 0–7 min. Then, the solution was removed carefully. Subsequently, 0.1 wt% TMC organic (n-hexane) solution was poured on the membrane surface for 0–2 min. Then, the membranes were kept in the oven (60 ℃, 10 min) to facilitate the IP reaction. Finally, the membrane was placed in deionized water over 24 h. A detailed fabrication scheme for the PEI/AMN-TMC membrane is shown in Fig. 1. The fabricated nanofiltration membranes with the relevant content of AMN, PEI, deposition time, and reaction time are shown in Table S1.

2.3. Membrane characterization

A NEXUS670 Fourier transform infrared spectrometer (FT-IR, ThermoFisher, USA) and X-ray photoelectron spectroscopy (XPS, PerkinElmer) were used to study the surface functional groups and element

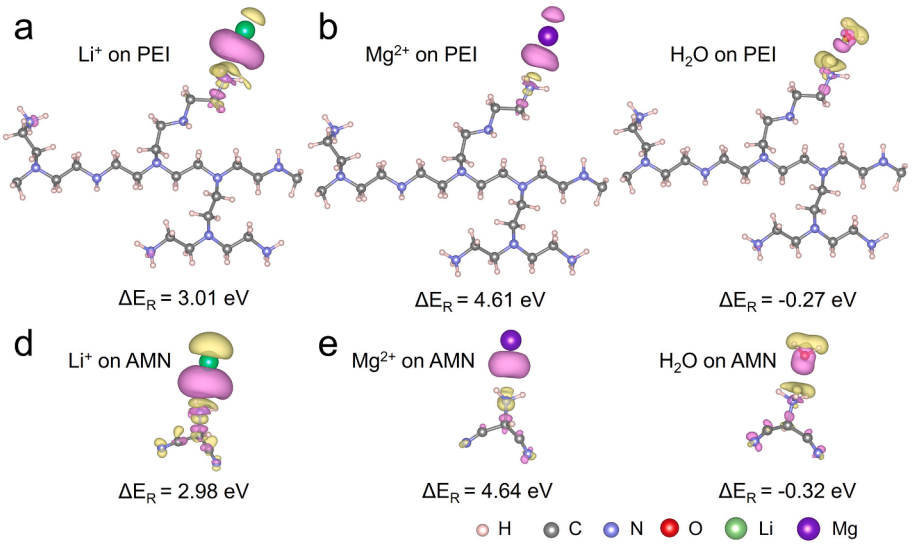

Fig. 2. DFT calculations for the repulsion energy between different molecules with cations and H_2O. Side illustration of the 3D electron density difference distribution of: Li^+; Mg^{2+} and H_2O on the $–NH_3^+$ of PEI (a, b, c) and AMN (d, e, f) as well as the corresponding the repulsion energy ΔE_R. Gray, blue, white, red, green, and purple balls represent carbon, nitrogen, hydrogen, oxygen, lithium, and magnesium, respectively. (For interpretation of the references to colour in this figure legend, the reader is referred to the web version of this article.)

information of the fabricated membranes, respectively. A Philips XL30 FEG scanning electron microscope (SEM, the Netherlands) was applied to inspect the morphology of the fabricated membranes. Metal was deposited on the membrane surface to improve the electro-conductivity of membrane before SEM observation. The surface information and the roughness of the fabricated membranes were evaluated by the Dimension Icon SPM atomic force microscope (AFM, Veeco Instruments Inc., USA). A contact angle meter (OCA20, Dataphysics Instruments, Germany) was employed to assess the hydrophilicity and hydrophobicity of the membranes. The charge properties of the fabricated membrane surface were evaluated by an electrokinetic analyzer (SurPASS 3, Anton Paar, Austria). In the pursuit of characterizing pore size distribution, the composition of feed solutions was varied, specifically employing solutions containing 200 ppm polyethylene glycols (PEGs) with molecular weights ranging from 200 g/mol to 2000 g/mol. The quantification of dissolved organic carbon was conducted using a total organic carbon (TOC) analyzer (Multi N/C 2100, Analytikjena). The pore size distribution of the membrane was subsequently determined by calculating the rejections of PEGs with the equation [26]:

$$\frac{dR(d_p)}{dd_p} = \frac{1}{d_p \ln\sigma_p \sqrt{2\pi}} exp\left[-\frac{(\ln d_p - \ln\mu_p)^2}{2(\ln\sigma_p)^2}\right] \quad (1)$$

where d_p, μ_p, and σ_p are the stokes diameter (nm), mean pore radius (nm) and the geometric standard deviation of the PEGs.

2.4. Separation performance tests

The separation performance of the membranes was assessed with a cross-flow filtration apparatus. The effective area for nanofiltration was 7.1 cm^2. All membranes were compacted at 6 bar for 30 min until the water permeance was stable before the formal test. The nanofiltration performance of membrane was estimated by the rejection (R) and permeability (P):

$$R(\%) = (1 - \frac{C_p}{C_f}) \times 100 \quad (2)$$

$$P = V/(A \times \Delta t \times \Delta p) \quad (3)$$

where V is the volume (L) of the permeance solution; A is the effective separation area (m^2); Δt is the interval time (h), and Δp is the operational pressure (bar); C_p and C_f represent the concentration (g/L) of permeate and feed solution, respectively.

The separation performance of all membranes for Mg^{2+}/Li^+ was assessed by separating mixed solutions of Mg^{2+}/Li^+ with different Mg^{2+}/Li^+ ratios from 5 to 50 (concentration: 2 g/L). The Mg^{2+}/Li^+ separation factor (S_{Mg^{2+}/Li^+}) was calculated by the salt concentrations of the permeate and feed solution based on the following equation [27,28]:

$$S_{Mg^{2+}/Li^+} = \frac{C_{Li^+p}/C_{Mg^{2+}p}}{C_{Li^+f}/C_{Mg^{2+}f}} \quad (4)$$

where $C_{Mg^{2+}f}$, C_{Li^+f} and $C_{Mg^{2+}p}$, C_{Li^+p} represent the concentrations of Mg^{2+} and Li^+ in the permeate and feed solutions, respectively.

2.5. Stability, anti-scaling, and anti-bacterial performance evaluation

The membrane stability was surveyed by a long-term testing. The stability of the membrane was estimated by testing the water permeance and separation factor of $MgCl_2$/LiCl mixed solution (2000 ppm, 6 bar) for seven days.

To investigate the anti-scaling properties of the membrane, a mixture solution containing 300 ppm Na_2SiO_3, 500 ppm $CaSO_4$, 500 ppm $MgCl_2$, and 500 ppm LiCl was prepared (pH 6.6 ± 0.1, 25 ℃) [16]. The anti-scaling testing was based on decreased normalized water permeance during filtration. Specifically, the above-mentioned scaling solution was filtered with the modified membrane at 6 bar for 30 h. The membrane was rinsed with NaOH solution (0.1 mM) carefully, and then the scaling solution was filtered again. Finally, the anti-scaling properties of the membranes were evaluated by comparing their normalized flux drop and recovery.

The evaluation of antibacterial robustness in membranes typically involves using *Escherichia coli (E. coli)* as the test microorganism. Prior to the start of the experiment, a 2.5 cm^2 test specimen is sterilized using 75 % ethanol and then dried for use. *E. coli* cells were cultured overnight in 5 ml Luria-Bertani broth (LB) media, shaking at 37 °C. The next morning, 1 ml of the overnight culture is inoculated into 50 ml prewarmed LB and allowed to grow for 2–3 h at 37 °C with shaking until reaching an optical density (OD600) of 0.5–1, equivalent to approximately 10^8 colony forming units (CFU) /mL. Subsequently, 5 ml of the cultured cell suspension is brought into full contact with the membrane (2.5 cm × 2.5

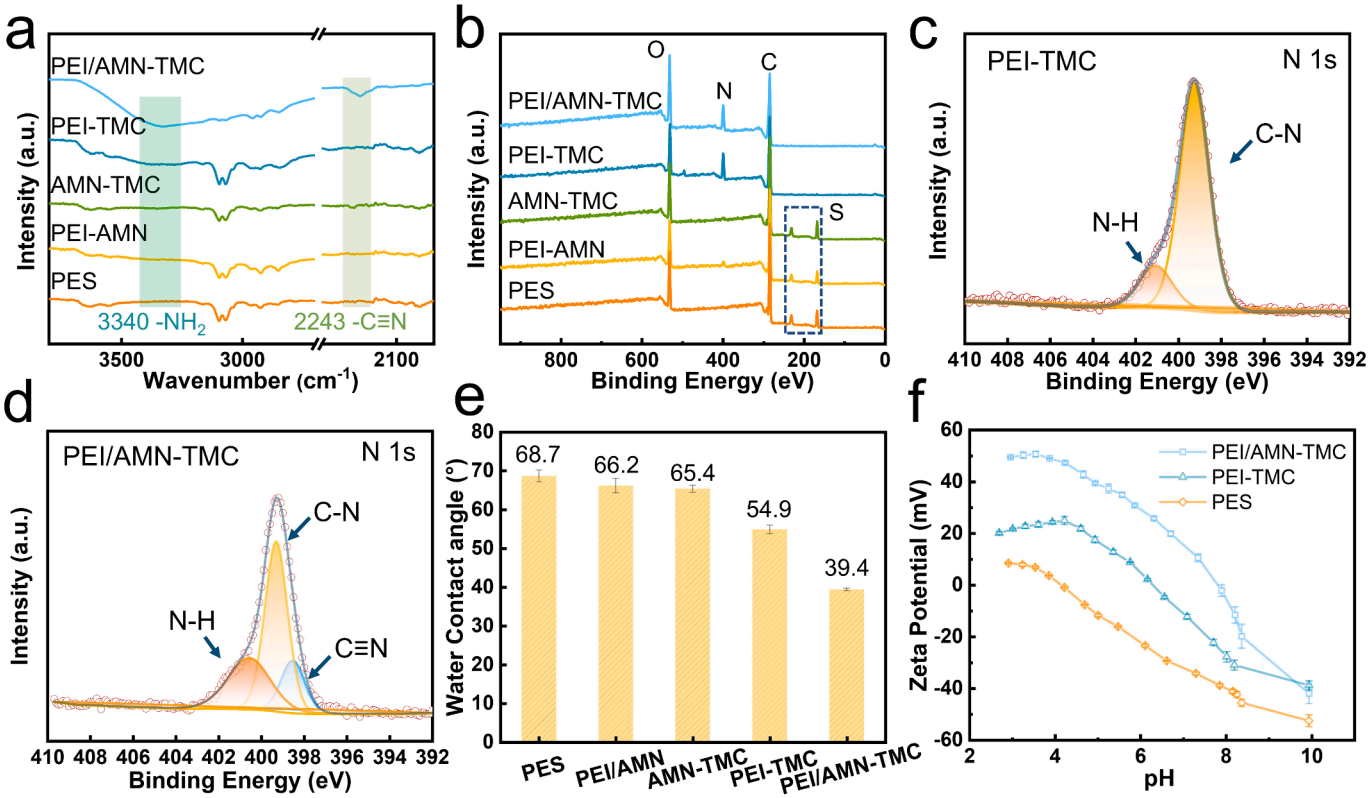

Fig. 3. (a) FT-IR spectra and (b) XPS wide-scan spectra of membranes. Core-level XPS spectra of N 1 s: (c) PEI-TMC membrane and (d) PEI/AMN-TMC membrane. (e) Water contact angle and (f) Zeta potential measurements of membranes.

cm), and cocultured at 37 °C and 200 rpm for 3 h. Following coculturing, a tenfold dilution series of the *E. coli* cells is plated on LB agar plates and incubated overnight at 37 °C. Images are captured using a scanner, and the number of colonies on each plate is determined, with plate counts ranging from 30 to 1000 CFU. The survival rate of cells in the control group is recorded as 100 %. The antibacterial efficiency of the membrane is calculated using the formula:

$$R = \frac{N_0 - N}{N_0} \times 100\% \quad (5)$$

where N_0 is the initial number of live bacteria in the control group (without membrane treatment), and N is the number of live bacteria upon membrane treatment. All experiments are conducted with three biological replicates to ensure the reliability and reproducibility of the results.

2.6. Density functional theory method

DFT were applied under the generalized gradient approximation (GGA) with the Perdew-Burke-Ernzerhof (PBE) function. The ultrasoft pseudopotentials were used for nuclei and core electrons. The plane-wave basis set with a kinetic energy cutoff (30 Ry) and a charge-density cutoff (300 Ry). The k-point mesh of 1 × 1 × 1 was used for the Brillouin zones. The models of AMN and PEI had been relaxed before calculating, as shown in Fig. S1. The vacuum layer was set with ~10 Å to remove the interaction from the slabs at z-direction. By adding the proton on the $–NH_2$ group of AMN and PEI, and the geometry structures were optimized again, the protonated AMN and PEI were obtained (shown in Fig. S2). In addition, the repulsion energy (ΔE_R) was calculated by Equation (6) [29]:

$$\Delta E_R = E_{total} - E_{adsorbate} - E_{molecule} \quad (6)$$

where E_{total} is the total energy of the compound, $E_{adsorbate}$ is the energy of adsorbate, and $E_{molecule}$ is the energy of the corresponding molecule. The DFT calculations were carried out by the PW modules in the Quantum ESPRESSO distribution [30].

3. Results and discussion

3.1. DFT prediction of molecules for Mg^{2+}/Li^+ separation membrane

DFT calculation was used to investigate the performance of PEI and AMN molecules on Mg^{2+}/Li^+ separation (Fig. 2 and Fig. S1-S4). The repulsion energy (ΔE_R) of ions by molecules was utilized as a descriptor of their repulsion capability [29]. First of all, models of AMN and PEI molecules were constructed and optimized as the initial phase (Fig. S1). Subsequently, the protonated AMN and PEI were optimized by adding the proton on the $–NH_2$ group to simulate protonated molecules in aqueous, as shown in Fig. S2. As shown in Fig. 2a and 2d, the $–NH_3$ functional group of AMN has a lower repulsion (2.98 eV) to Li^+ than that of PEI (3.01 eV), suggesting that AMN is more conducive to the transport of Li^+. Simultaneously, the repulsion energy of Mg^{2+} on the $–NH_3$ group of AMN (4.64 eV) is greater than that of PEI (4.61 eV), indicating that AMN is more conducive to the rejection of Mg^{2+} (Fig. 2b and 2e). Meanwhile, the water repulsion of AMN is lower than that of PEI (Fig. 2c and 2f), indicating that AMN has a better hydrophilicity. Fig. 2 presents the electron density difference illustrating the interactions of Li^+, Mg^{2+} and H_2O adsorption in the presence of AMN and PEI. As depicted in the Fig. 2, compared to PEI, AMN induces noticeable charge redistribution. It is evident that AMN exhibits a stronger affinity for Li^+ and H_2O, resulting in enhanced interactions with these species. Simultaneously, the interaction between AMN and Mg^{2+} is comparatively weaker, indicating a greater repulsion between them, consistent with the calculated repulsion energy results. In addition, the -C≡N group of AMN also shows the stronger repulsion to Mg^{2+} compared to the $–NH_3^+$ group of PEI (4.77 vs. 4.61 eV) and the lower repulsion to Li^+ (2.63 vs. 3.01

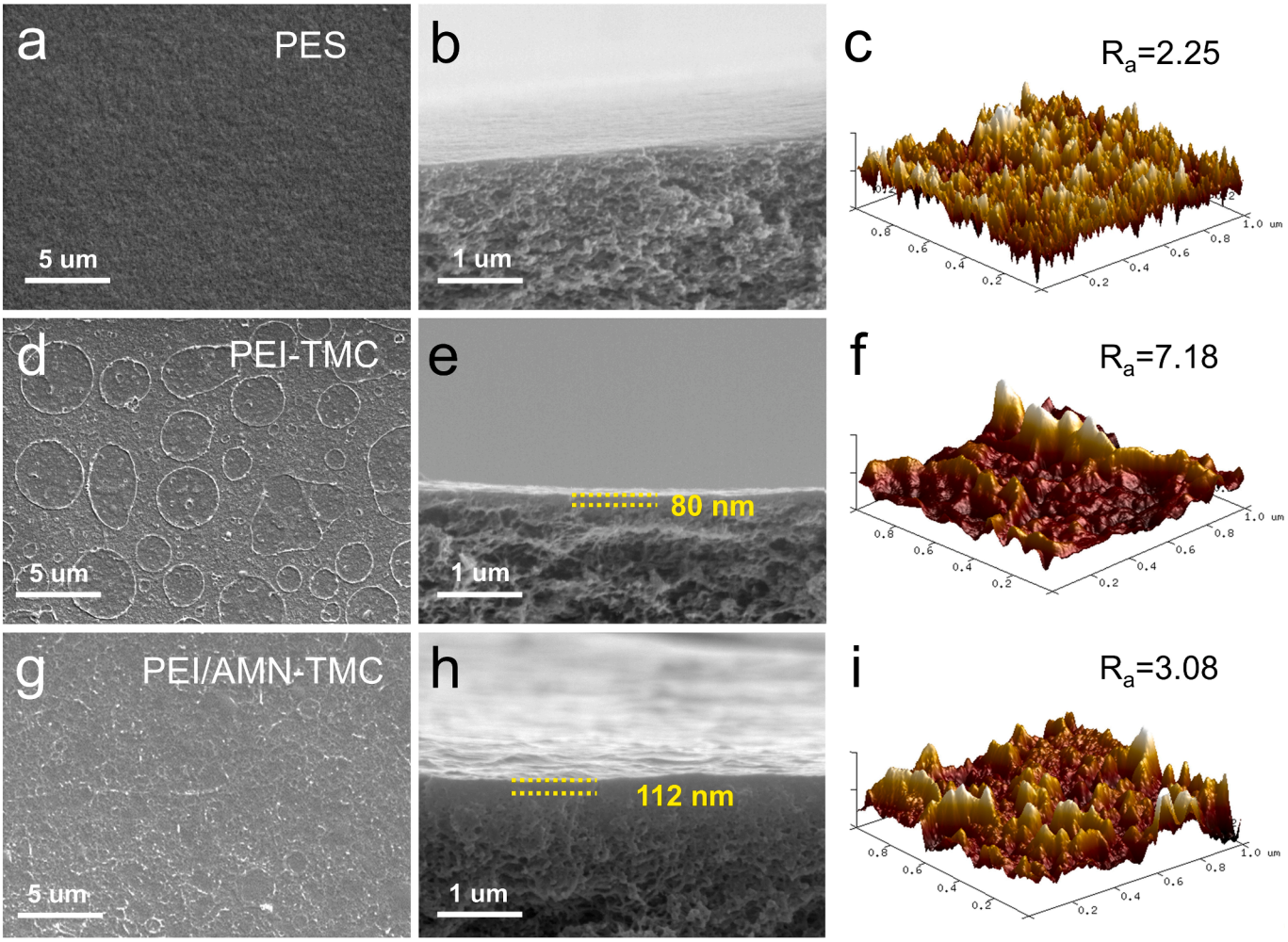

Fig. 4. Surface and cross-sectional morphologies of (a, b) PES, (d, e) PEI-TMC and (g, h) PEI/AMN-TMC membrane, respectively. The AFM images of (c) PES, (f) PEI-TMC and (i) PEI/AMN-TMC membrane.

eV), suggesting its better selectivity to Li^+ (Fig. S4). Therefore, not only the protonated $–NH_3^+$ group of AMN has better selectivity to Li^+ than the protonated $–NH_3^+$ group of PEI, but the -C≡N group of AMN also shows better selectivity to Li^+. The above results clearly show that the AMN molecule is more repellent to Mg^{2+}, has more affinity to Li^+ and has better hydrophilicity, which has been confirmed to have a particular potential in separating Mg^{2+} and Li^+ at the molecular level.

3.2. Characterization of membranes

The chemical composition of the membrane surface was explored by FT-IR, as shown in Fig. 3a and S5. As shown in Fig. 3a and S5, the stretching vibration of the $–NH_2$ group near 3340 cm^{-1} and the deformation vibration near 1630 cm^{-1} appear in the spectra of PEI/AMN-TMC and PEI-TMC, which may be attributed to many $–NH_2$ groups of PEI/AMN-TMC and PEI-TMC membranes [31,32]. Interestingly, the spectra of the PEI/AMN-TMC membrane showed additional wagging vibrations and twisting vibrations of $–NH_2$ groups at 1124 cm^{-1} and 1030 cm^{-1}, which were attributed to the $–NH_2$ group of AMN (Fig. S5c), indicating that AMN is stably embedded between PEI chains and rarely reacts with TMC [32]. It is worth noting that the vibration of the -C≡N groups (~2243 cm^{-1}) is clearly shown in the spectra of PEI/AMN-TMC, suggesting that the stable -C≡N groups did not react with PEI or TMC [27]. This observation further corroborates the stable integration of AMNs within the membrane structure. The absence of vibrational signals corresponding to $–NH_2$ and -C≡N groups in the spectra of PEI/AMN and the AMN-TMC membrane indicates the absence of a dense membrane formation. This indicates that the co-deposition of AMN and PEI does not lead to membrane formation, and AMN cannot react as monomer with TMC to form a membrane. Consequently, the attachment of PEI and AMN onto the PES substrate is challenging, resulting in the limited visibility of their $–NH_2$ and -C≡N groups in the spectra.

The presence of S element can be observed in the XPS wide scan spectra of PES, AMN-TMC and PEI/AMN membranes (Fig. 3b). This is consistent with the absence of dense nanofiltration membrane formation on the PES substrate, consistent with the results of FT-IR analysis. In addition, non-negligible N elements were detected on the PEI/AMN membrane surface, indicating that a small amount of PEI and AMN remained on the membrane surface, which confirmed that they did not co-deposit to form a dense membrane. To further explore the cause of N element vibration of PEI-TMC and PEI/AMN-TMC membranes, the core-level XPS spectra of N 1 s are displayed in Fig. 3c and 3d. A new characteristic peak of the -C≡N group appears in the N 1 s core-level spectra of the PEI/AMN-TMC, suggesting that it is present in the membrane in a stable way, which is consistent with the results of the FT-IR analysis. This proves that AMN has not reacted with TMC during membrane formation and becomes embedded in the membrane structure.

The water contact angle of a membrane is an important parameter for assessing its hydrophilicity. In Fig. 3e, we present the water contact angles for the PES, AMN-TMC, PEI/AMN, PEI-TMC, and PEI/AMN-TMC membranes. It is evident that PES, AMN-TMC, and PEI/AMN membranes exhibit similar water contact angles. This similarity can be

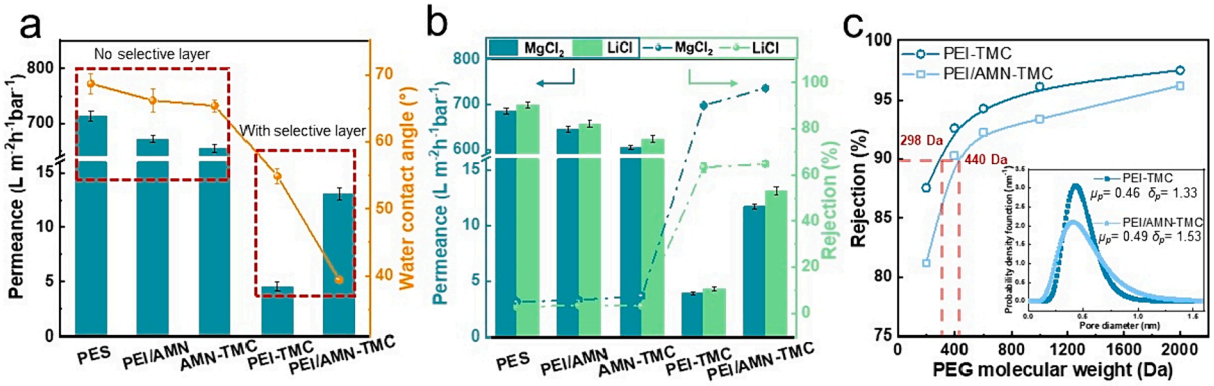

Fig. 5. (a) Pure water permeance and water contact angle of fabricated membranes. (b) Salt solution permeance and rejection of fabricated membranes. (c) Molecular weight cut-off and pore size distribution.

attributed to the absence of dense membranes on the AMN-TMC and PEI/AMN samples, which is consistent with the above analysis. On the other hand, the water contact angle of the PEI/AMN-TMC is smaller than the PEI-TMC, suggesting the embedded AMN improve the hydrophilicity of the PEI/AMN-TMC membrane, and also confirms that AMN molecules are more hydrophilic, which is consistent with the results of the DFT analysis. The enhancement of hydrophilicity yields a higher water permeance and a rapid mass transfer through the membrane.

The zeta potential of the membrane surface was analyzed to assess its charge (as depicted in Fig. 3f). Significantly, the zeta potential of the PEI-TMC membrane was considerably higher than that of the unmodified PES membrane at the same pH. This variation can be attributed to the protonation of numerous amino groups in PEI, resulting in an increased positive charge on the surface. Moreover, the introduction of AMN with amino groups in the AMN-modified PEI/AMN-TMC membrane led to an even higher zeta potential. This suggests that the addition of AMN enhances the repulsion of positively charged ions, further amplifying the overall positive charge on the membrane.

The SEM and AFM were employed to analyze the surface morphology of the PES, AMN-TMC, PEI/AMN, PEI-TMC, and PEI/AMN-TMC membranes. The surfaces and cross-sectional morphologies of the fabricated nanofiltration membranes are illustrated in Fig. 4, S6, and S7. The surface image of the pristine PES membrane, which exhibits a flat surface (Fig. 4a), consistent with the findings in the literature [2]. According to the literature [11], the reaction of PEI with TMC leads to the formation of disk-like patterns on the PEI-TMC membrane (Fig. 4d). An SEM image of the PEI/AMN-TMC membrane surface is presented in Fig. 4g. Remarkably, the densely distributed disk-like structures on the membrane surface imply that the intercalation of AMN between PEI chains influences the reaction between PEI and TMC. It is well established that, during interfacial polymerization, the rates of molecular diffusion and chemical reaction are two pivotal factors that influence the surface morphology of thin membranes [33]. The cross-sectional morphology of the PEI-TMC and PEI/AMN-TMC membranes as shown in Fig. 4e and 4 h. In the cross-sectional view, clear polyamide layers are evident in both the PEI-TMC and PEI/AMN-TMC membranes. The active layer thickness of the PEI-TMC membrane is ~ 80 nm, in close agreement with the thickness reported in the literature [17]. Notably, the polyamide layer in the PEI/AMN-TMC membrane measures ~ 112 nm, which is greater than that of the PEI-TMC membrane (~80 nm) (Fig. 4h). This may be because the AMN molecules embedded between PEI molecules expand the space between PEI molecules and are conducive to the diffusion of PEI molecules. Therefore, the thickness of the formed active layer is increased, and the structure of the polyamide layer is looser, which also contributes to the rapid mass transfer. According to the AFM images (Fig. 4f and 4i), the surface average roughness (Ra = 3.08 nm) of the PEI/AMN-TMC membrane is lower than that of the PEI-TMC membrane (7.18 nm). This observation indicates that AMN molecules influence the diffusion of PEI molecules, resulting in a smoother surface for the PEI/AMN-TMC membrane, which may contribute to its excellent anti-scaling properties. Furthermore, both the surface and cross-sectional morphology of AMN-TMC and PEI/AMN closely resemble PES (as shown in Fig. S6 and S7), providing evidence that no polyamide layer has formed on the surface, in alignment with the previous characterization results.

3.3. Optimization of membrane fabrication conditions

A comprehensive overview of the H_2O permeance of the membranes fabricated by various parameters as shown in Fig. 5a and S6-S9. The water permeance of PES, AMN-TMC, and PEI/AMN membranes is comparable, as depicted in Fig. 5a. This observation suggests that AMN-TMC and PEI/AMN membranes lack a dense selective layer on their surfaces, aligning with the water contact angle analysis and other characterization outcomes. On the other hand, the incorporation of AMN significantly enhanced the pure water permeance of the membrane with selective layer, corresponding to a smaller water contact angle (Fig. 5a). This improvement can be attributed to AMN embedded within the membrane structure. As shown in Fig. S8, the pure water permeance progressively increases with the concentration of AMN. This can be attributed to the notion that more embedded AMN leads to a looser membrane structure, resulting in a higher pure water permeance. The concentration of PEI in the aqueous phase solution is also considered as an important factor. As illustrated in Fig. S9, an increase in the concentration of PEI leads to a decrease in pure water permeance, dropping from 14.3 $L{\cdot}m^{-2}{\cdot}h^{-1}{\cdot}bar^{-1}$ to 8.3 $L{\cdot}m^{-2}{\cdot}h^{-1}{\cdot}bar^{-1}$. This can be attributed to the higher presence of PEI molecules, resulting in a denser membrane structure. To optimize the water permeance of the membrane, the deposition time of the mixed solution containing PEI and AMN molecules on the membrane was examined (Fig. S10). The pure water permeance decreased from 13.8 $L{\cdot}m^{-2}{\cdot}h^{-1}{\cdot}bar^{-1}$ to 9.5 $L{\cdot}m^{-2}{\cdot}h^{-1}{\cdot}bar^{-1}$ with the increase of deposition time, which may be due to the deposition of more PEI and AMN molecules to obtain a denser membrane. Finally, the reaction times of TMC with PEI and AMN in the aqueous phase were examined, as shown in Fig. S11. It was observed that longer reaction times resulted in a decrease in water permeance. This can be attributed to the formation of a denser polyamide layer as the reaction time is extended.

The optimization of permeance and rejection for five salt solutions ($MgCl_2$, $MgSO_4$, Na_2SO_4, NaCl, and LiCl) with 1000 ppm was achieved by preparing membranes under various experimental conditions (Fig. 5b and S12-16). The permeance of each salt solution has a similar trend with permeance of pure water under the corresponding changing conditions. Specifically, the membrane permeance exhibited an upward trend with increasing AMN concentration, while it decreased with increasing PEI concentration, deposition time, and reaction time.

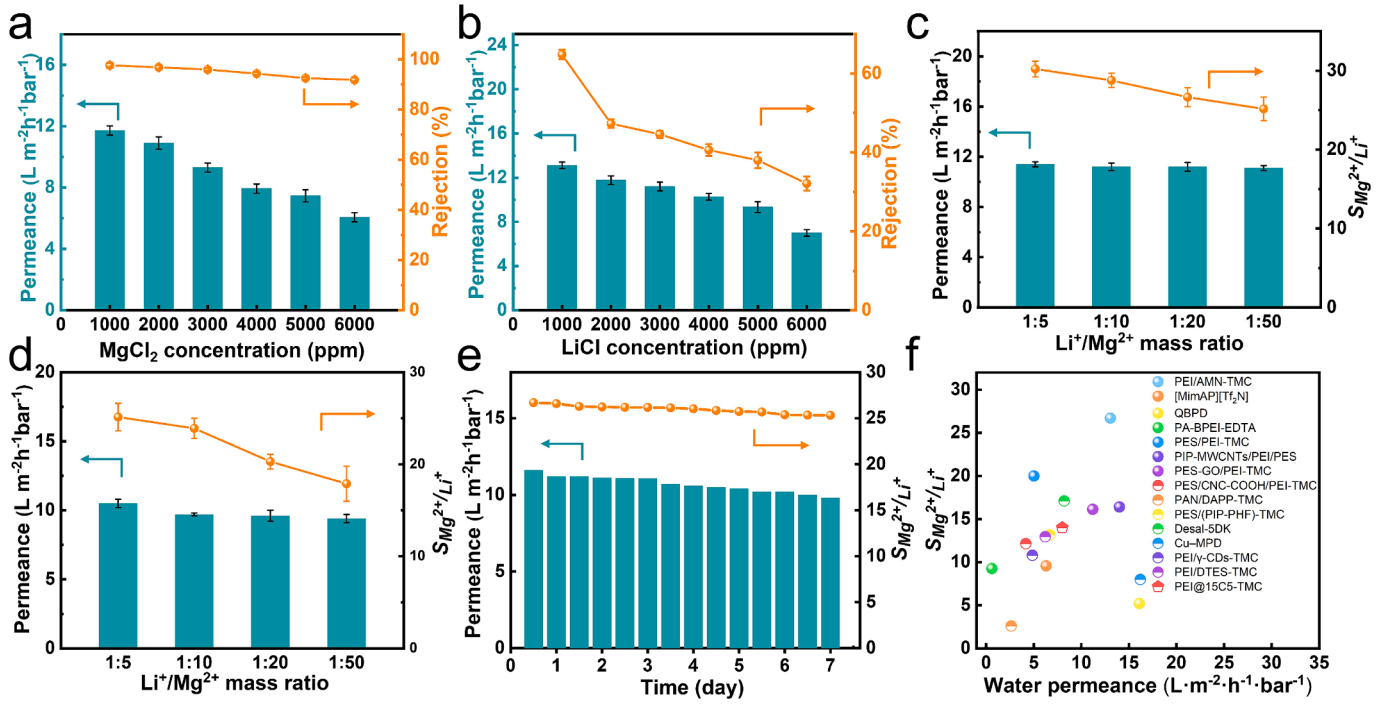

Fig. 6. Separation performance of PEI/AMN-TMC membrane. Permeance and rejection to (a) $MgCl_2$ and (b) LiCl with different feed solution concentrations. Effect of different Mg^{2+}/Li^+ mass ratios on the permeance and S_{Mg^{2+}/Li^+} for (c) 2000 ppm and (d) 3000 ppm. (e) Long-term stability at 6 bar (2000 ppm, $Mg^{2+}/Li^+ = 20{:}1$). (f) Comparative separation factors (S_{Mg^{2+}/Li^+}) and water permeance of the PEI/AMN-TMC membrane and reported positively charged membranes. (Detailed data in Table S2).

Fig. S13 also illustrates that as the concentration of AMN increases, the rejection of each salt solution initially rises and then declines. The increase in salt solution rejection can be attributed to the presence of AMN, which introduces additional positive charges from protonated $–NH_2$ (as concluded from zeta potential measurements). The decrease in rejection rate could be attributed to an excessive number of AMN molecules, which results in a looser membrane structure. This observation further supports the notion that AMN molecules intercalate between PEI chains, creating a larger space that causes a looser membrane structure. Furthermore, as the PEI concentration, deposition time, and reaction time increase, the salt rejection initially increases and reaches a stable state. The enhanced rejection can be attributed to the formation of denser or more positively charged membranes. However, it should be noted that membranes with similar salt rejection have a lower water permeance as the reaction conditions become more intense. Therefore, the optimal reaction conditions for the AMN-modified PEI-TMC membrane are as follows: AMN concentration of 0.7 wt%, PEI concentration of 0.5 wt%, deposition time of 5 min, and reaction time of 1 min.

3.4. Separation performance of PEI/AMN-TMC nanofiltration membrane

To assess the selectivity of the PEI/AMN-TMC for Li^+ at different concentrations, the filtration performance was examined for different concentrations of $MgCl_2$ and LiCl. As depicted in Fig. 6a, b, the salt solution permeance of the membrane was found to show a reasonably linear decrease with increasing salt concentration. This can be attributed to the decreased mass transfer driving force due to the elevated osmotic pressure and significant concentration polarization. Furthermore, although the $MgCl_2$ rejection exhibited a slight decrease, it remained above 91.8 %; on the other hand, the rejection of LiCl dropped to 32.1 %. The diminished repulsion at higher salt concentrations can be attributed to the reduction in positive charge of membrane, resulting in a weakened electrostatic repulsion due to enhanced screening by the numerous counterions in the solution. Nevertheless, PEI/AMN-TMC membrane still has great potential for high-concentration Mg^{2+}/Li^+ mixed solutions.

Mg^{2+}/Li^+ mixed solutions with different mass ratios were employed to estimate the selectivity of PEI/AMN-TMC membranes at different Mg^{2+}/Li^+ ratios. In the feed solution with a total concentration of 2000 ppm for the simulated brine, the S_{Mg^{2+}/Li^+} values were calculated to be 30.2, 28.7, 26.6, and 25.1 when the mass ratios of Mg^{2+}/Li^+ were 5, 10, 20, and 50, respectively (Fig. 6c). The separation factor exhibited minimal changes with the increased Mg^{2+}/Li^+ mass ratio. Therefore, PEI/AMN-TMC membranes have great potential for high Mg^{2+}/Li^+ ratio brine of salt lakes worldwide. Evaluation of the separation performance of PEI/AMN-TMC in high concentration salt solution is helpful to explore its possibility in practical application. The S_{Mg^{2+}/Li^+} value only decreased to 20.3 and 19.0 with the concentration of Mg^{2+}/Li^+ mixed solution were raised to 3000 and 4000 ppm (Fig. 6d and S17). Similar to the mono-salt solutions, the presence of high concentrations of Cl^- ions neutralizes the positive charges from the membrane. Consequently, the Donnan effect of the membrane on Mg^{2+} is weakened, leading to a reduction of the Li^+ selectivity. Moreover, the PEI/AMN-TMC membrane exhibited a stable separation throughout a continuous filtration test conducted over a period of 7 days (Fig. 6e). This remarkable stability can be attributed to the presence of a stable positively charged moiety, underscoring the excellent stability of the PEI/AMN-TMC membrane. Furthermore, the PEI/AMN-TMC membrane maintains an excellent separation factor while retaining high permeance compared to nanofiltration membranes documented in the literature (as depicted in Fig. 6f and detailed in Table S2), highlighting its substantial potential for various applications.

3.5. Anti-scaling and anti-bacterial performances of PEI/AMN-TMC membrane

Scaling of membranes by inorganic pollutants is a significant concern in lithium extraction from salt lakes. During the separation process, the membrane surface is susceptible to scaling by inorganic pollutants, leading to a decline in its separation performance. Therefore, the

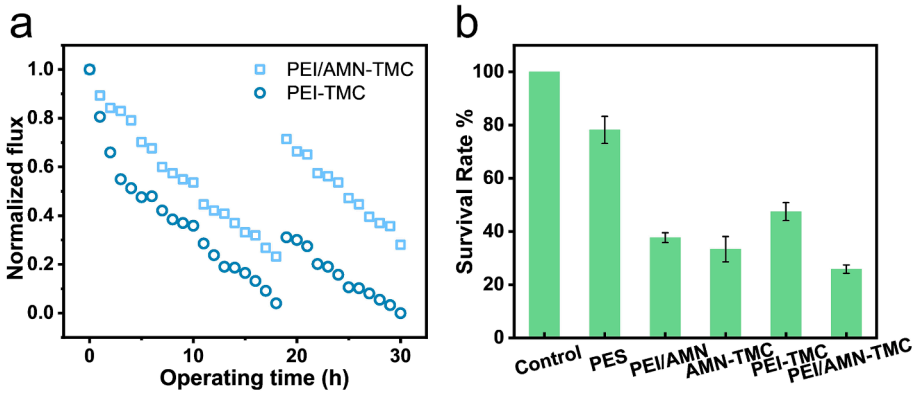

Fig. 7. (a) Representative normalized flux decline curves of membrane testing with scaling solution. (b) The quantified anti-bacterial ability of membranes.

membrane's ability to resist scaling is a crucial parameter to consider. To evaluate the membrane's ability to resist inorganic fouling, a simulated scaling solution containing scale-forming ions such as Ca^{2+}, SiO^{3-}, and SO_4^{2-} was utilized. As depicted in the Fig. 6f, the flux of the PEI-TMC membrane decreased by over 90 % with the increase in scaling time. In contrast, the PEI/AMN-TMC membrane showed a significantly higher flux than the PEI-TMC membrane after 18 h. Additionally, after cleaning, the recoverable flux of the PEI/AMN-TMC membrane was considerably higher than that of the PEI-TMC membrane (Fig. 7a). These findings further confirm the excellent ability of the PEI/AMN-TMC membrane to resist inorganic scaling.

Simultaneously, the PEI/AMN-TMC membrane exhibits excellent anti-bacterial properties, indicating its effectiveness in preventing biological fouling. Compared with the PEI-TMC, the AMN-TMC and PEI/AMN had a better anti-bacterial performance, which was derived from the excellent anti-bacterial ability of AMN (Fig. 7b and S18-S19). Furthermore, the colony-forming unit data showed that the viability of *E. coli* on PEI/AMN-TMC membranes with AMN was significantly reduced to 25.8 %. This feature further enhances its suitability for large-scale applications.

The PEI/AMN-TMC membrane exhibits enhanced hydrophilicity, allowing for the formation of a stable hydration layer on its surface. This characteristic contributes to a reduction in inorganic scaling and biological fouling. Membranes with higher hydrophilicity possess a more significant energy barrier against the nucleation of pollutants, thereby minimizing scaling and biological fouling on the membrane surface [33]. Additionally, the PEI/AMN-TMC has a lower roughness than PEI-TMC membranes. The smooth surface of the PEI/AMN-TMC membrane reduces the adhesion sites for pollutants, further enhancing its anti-scaling and anti-bacterial properties. Consequently, the hydrophilicity and reduced roughness render the PEI/AMN-TMC highly effective in preventing inorganic scaling and anti-bacterial.

3.6. DFT calculation of small molecules embedded mechanism

DFT calculations were employed to validate the reliability of embedding AMN molecules between PEI molecular chains. The results clearly indicate that introducing AMN molecules leads to expanding the space between PEI chains (Fig. S20). This enlarged space between the PEI chains promotes efficient mass transfer, aligning with the proposed mechanism. Additionally, the calculation of the binding energy (-0.93 eV) demonstrates the stable embedding of AMN molecules within the PEI matrix, ensuring the membrane's stability. In summary, DFT analysis confirms that AMN molecules can be securely intercalated between PEI chains, resulting in a looser PA layer and facilitating rapid mass transfer in the nanofiltration process.

4. Conclusion

In conclusion, a straightforward method for controlling the structure of polyamide membranes was introduced, by incorporating AMN, small molecules derived from prebiotic chemistry, between PEI chains. This approach allows efficient lithium extraction from high Mg^{2+}/Li^+ ratio salt solutions while significantly improving water permeation. The incorporation of AMNs not only increases the space between PEI chains but also enhances their hydrophilicity, resulting in reduced barriers to water transport. The resulting PEI/AMN-TMC membrane has an excellent water permeance of 13.1 $L{\cdot}m^{-2}{\cdot}h^{-1}{\cdot}bar^{-1}$ and high $MgCl_2$ rejection of 97.53 % with long-term stability. Moreover, The membrane exhibits exceptional performance in recovering lithium from model salt lake brine solutions. It effectively reduces the highly concentrated Mg^{2+}/Li^+ ratio from 20 to 0.8 during the separation process, resulting in a high S_{Mg^{2+}/Li^+} value of 26.7. These results indicate the membrane's potential for effectively recovering lithium from the brine of salt lakes. Furthermore, the intercalated AMN molecules confer the membrane with exceptional anti-scaling and anti-bacterial properties. Additionally, DFT calculations have validated the enhanced Li^+ selectivity and hydrophilicity of AMN molecules and confirmed their stable intercalation between PEI chains. This research provides valuable insights into the design of functionalized nanofiltration membranes with improved water permeance and ion selectivity, offering potential applications in various water treatments.

CRediT authorship contribution statement

Junwei Li: Writing – original draft, Methodology, Investigation, Data curation, Conceptualization. **Long Fang:** Methodology, Investigation. **Daliang Xu:** Resources, Investigation, Data curation. **Xi Zhang:** Formal analysis, Data curation. **Lei Jiang:** Investigation, Formal analysis. **Qingjuan Zhu:** Methodology, Formal analysis. **Qin Chen:** Investigation, Formal analysis. **Pengrui Jin:** Investigation, Formal analysis. **Alexander Volodine:** Methodology. **Raf Dewil:** Supervision. **Xiahui Gui:** Writing – review & editing, Resources. **Qieyuan Gao:** Writing – review & editing, Supervision, Methodology, Conceptualization. **Bart Van der Bruggen:** Writing – review & editing, Supervision, Project administration, Funding acquisition.

Declaration of competing interest

The authors declare that they have no known competing financial interests or personal relationships that could have appeared to influence the work reported in this paper.

Data availability

No data was used for the research described in the article.

Acknowledgments

This work was supported by the National Nature Science Foundation of China (Grant No. 52300083 and No. 52174265) and Postdoctoral Fellowship Program of CPSF (No. GZB20230965). Junwei Li and Qieyuan Gao would like to acknowledge the support provided by China Scholarship Council (CSC) of the Ministry of Education, P.R. china (CSC no. 202108350006 and no. 202006420004). We thank the technical supporting from Christine Wouters and Herman Tollet for this work.

Appendix A. Supplementary data

Supplementary data to this article can be found online at https://doi.org/10.1016/j.cej.2024.150659.

References

[1] H. Luo, H. Peng, Q. Zhao, High flux Mg2+/Li+ nanofiltration membranes prepared by surface modification of polyethylenimine thin film composite membranes, Appl. Surf. Sci. 579 (2022) 152161, https://doi.org/10.1016/j.apsusc.2021.152161.
[2] L. Wang, D. Rehman, P.F. Sun, A. Deshmukh, L. Zhang, Q. Han, Z. Yang, Z. Wang, H.D. Park, J.H. Lienhard, C.Y. Tang, Novel Positively Charged Metal-Coordinated Nanofiltration Membrane for Lithium Recovery, ACS Appl. Mater. Inter. 13 (14) (2021) 16906–16915, https://doi.org/10.1021/acsami.1c02252.
[3] Y. Zhao, M. Wu, P. Shen, C. Uytterhoeven, N. Mamrol, J. Shen, C. Gao, B. Van der Bruggen, Composite anti-scaling membrane made of interpenetrating networks of nanofibers for selective separation of lithium, J. Membr. Sci. 618 (2021) 118668, https://doi.org/10.1016/j.memsci.2020.118668.
[4] Z.-Y. Ji, Q.-B. Chen, J.-S. Yuan, J. Liu, Y.-Y. Zhao, W.-X. Feng, Preliminary study on recovering lithium from high Mg2+/Li+ ratio brines by electrodialysis, Sep. Purif. Technol. 172 (2017) 168–177, https://doi.org/10.1016/j.seppur.2016.08.006.
[5] W. Wang, G. Hong, Y. Zhang, X. Yang, N. Hu, J. Zhang, P. Sorokin, L. Shao, Designing an energy-efficient multi-stage selective electrodialysis process based on high-performance materials for lithium extraction, J. Membr. Sci. 675 (2023) 121534, https://doi.org/10.1016/j.memsci.2023.121534.
[6] D. Shi, L. Zhang, X. Peng, L. Li, F. Song, F. Nie, L. Ji, Y. Zhang, Extraction of lithium from salt lake brine containing boron using multistage centrifuge extractors, Desalination 441 (2018) 44–51, https://doi.org/10.1016/j.desal.2018.04.029.
[7] D. Shi, B. Cui, L. Li, M. Xu, Y. Zhang, X. Peng, L. Zhang, F. Song, L. Ji, Removal of calcium and magnesium from lithium concentrated solution by solvent extraction method using D2EHPA, Desalination 479 (2020) 114306, https://doi.org/10.1016/j.desal.2019.114306.
[8] X. Liu, M. Zhong, X. Chen, Z. Zhao, Separating lithium and magnesium in brine by aluminum-based materials, Hydrometallurgy 176 (2018) 73–77, https://doi.org/10.1016/j.hydromet.2018.01.005.
[9] C. Guo, X. Qian, F. Tian, N. Li, W. Wang, Z. Xu, S. Zhang, Amino-rich carbon quantum dots ultrathin nanofiltration membranes by double "one-step" methods: Breaking through trade-off among separation, permeation and stability, Chem. Eng. J. 404 (2021) 127144, https://doi.org/10.1016/j.cej.2020.127144.
[10] H. Li, Y. Li, M. Li, Y. Jin, G. Kang, Y. Cao, Improving Mg2+/Li+ separation performance of polyamide nanofiltration membrane by swelling-embedding-shrinking strategy, J. Membr. Sci. 669 (2023) 121321, https://doi.org/10.1016/j.memsci.2022.121321.
[11] X. Zhang, J. Zheng, P. Jin, D. Xu, S. Yuan, R. Zhao, S. Depuydt, Y. Gao, Z.L. Xu, B. Van der Bruggen, A PEI/TMC membrane modified with an ionic liquid with enhanced permeability and antibacterial properties for the removal of heavy metal ions, J. Hazard. Mater. 435 (2022) 129010, https://doi.org/10.1016/j.jhazmat.2022.129010.
[12] Y. Li, S. Wang, W. Wu, H. Yu, R. Che, G. Kang, Y. Cao, Fabrication of positively charged nanofiltration membrane with uniform charge distribution by reversed interfacial polymerization for Mg2+/Li+ separation, Journal of Membrane Science 659 (2022) 120809, https://doi.org/10.1016/j.memsci.2022.120809.
[13] P. Xu, W. Wang, X. Qian, H. Wang, C. Guo, N. Li, Z. Xu, K. Teng, Z. Wang, Positive charged PEI-TMC composite nanofiltration membrane for separation of Li+ and Mg2+ from brine with high Mg2+/Li+ ratio, Desalination 449 (2019) 57–68, https://doi.org/10.1016/j.desal.2018.10.019.
[14] P. Xu, J. Hong, X. Qian, Z. Xu, H. Xia, Q.-Q. Ni, "Bridge" graphene oxide modified positive charged nanofiltration thin membrane with high efficiency for Mg2+/Li+ separation, Desalination 488 (2020) 114522, https://doi.org/10.1016/j.desal.2020.114522.
[15] Q. Bi, C. Zhang, J. Liu, X. Liu, S. Xu, Positively charged zwitterion-carbon nitride functionalized nanofiltration membranes with excellent separation performance of Mg2+/Li+ and good antifouling properties, Sep. Purif. Technol. 257 (2021) 117959, https://doi.org/10.1016/j.seppur.2020.117959.
[16] F. Soyekwo, H. Wen, D. Liao, C.K. Liu, Nanofiltration Membranes Modified with a Clustered Multiquaternary Ammonium-Based Ionic Liquid for Improved Magnesium/Lithium Separation, ACS Appl. Mater. Inter. 14 (28) (2022) 32420–32432, https://doi.org/10.1021/acsami.2c0365032420.
[17] Y. Xu, H. Peng, H. Luo, Q. Zhang, Z. Liu, Q. Zhao, High performance Mg2+/Li+ separation membranes modified by a bis-quaternary ammonium salt, Desalination 526 (2022) 115519, https://doi.org/10.1016/j.desal.2021.115519.
[18] B. He, H. Peng, Y. Chen, Q. Zhao, High performance polyamide nanofiltration membranes enabled by surface modification of imidazolium ionic liquid, J. Membr. Sci. 608 (2020) 118202, https://doi.org/10.1016/j.memsci.2020.118202.
[19] J. Li, X. Hu, G. Zhong, Y. Liu, Y. Ji, J. Chen, Z. Wen, A General Self-Sacrifice Template Strategy to 3D Heteroatom-Doped Macroporous Carbon for High-Performance Potassium-Ion Hybrid Capacitors, Nano-Micro Lett. 13 (1) (2021) 131, https://doi.org/10.1007/s40820-021-00659-7.
[20] X. Hu, G. Zhong, J. Li, Y. Liu, J. Yuan, J. Chen, H. Zhan, Z. Wen, Hierarchical porous carbon nanofibers for compatible anode and cathode of potassium-ion hybrid capacitor, Energy Environ. Sci. 13 (8) (2020) 2431–2440, https://doi.org/10.1039/d0ee00477d.
[21] Z. Pei, Q. Meng, L. Wei, J. Fan, Y. Chen, C. Zhi, Toward Efficient and High Rate Sodium-Ion Storage: A New Insight from Dopant-Defect Interplay in Textured Carbon Anode Materials, Energy Storage Mater. 28 (2020) 55–63, https://doi.org/10.1016/j.ensm.2020.02.033.
[22] Y. Li, M. Kong, J. Hu, J. Zhou, Carbon-Microcuboid-Supported Phosphorus-Coordinated Single Atomic Copper with Ultrahigh Content and Its Abnormal Modification to Na Storage Behaviors, Adv. Energy Mater. 2000400 (2020), https://doi.org/10.1002/aenm.202000400.
[23] L. Wang, B. Lu, S. Wang, W. Cheng, Y. Zhao, J. Zhang, X. Sun, Ultra-high performance of Li/Na ion batteries using N/O dual dopant porous hollow carbon nanocapsules as an anode, J. Mater. Chem. A 7 (2019) 11117–11126, https://doi.org/10.1039/c8ta12540f.
[24] P. Gao, P. Jin, R. Dumas, J. Huang, A.B. Asha, R. Narain, I. Vankelecom, B. Van der Bruggen, X. Yang, High-performance zwitterionic membranes via an adhesive prebiotic chemistry-inspired coating strategy: A demonstration in dye/salt fractionation, J. Membr. Sci. 676 (2023) 121572, https://doi.org/10.1016/j.memsci.2023.121572.
[25] Q. Gao, Q. Zhu, J. Zheng, S. Yuan, Y. Wang, R. Zhao, Y. Liu, X. Gui, C. Wang, A. Volodine, P. Jin, B. Van der Bruggen, Positively charged membranes for dye/salt separation based on a crossover combination of Mannich reaction and prebiotic chemistry, J. Hazard. Mater. 440 (2022) 129744, https://doi.org/10.1016/j.jhazmat.2022.129744.
[26] X. Zhu, X. Tang, X. Luo, Z. Yang, X. Cheng, Z. Gan, D. Xu, G. Li, H. Liang, Stainless steel mesh supported thin-film composite nanofiltration membranes for enhanced permeability and regeneration potential, J. Membr. Sci. 618 (2021) 118738, https://doi.org/10.1016/j.memsci.2021.118738.
[27] T. Gu, R. Zhang, S. Zhang, B. Shi, J. Zhao, Z. Wang, M. Long, G. Wang, T. Qiu, Z. Jiang, Quaternary ammonium engineered polyamide membrane with high positive charge density for efficient Li+/Mg2+ separation, J. Membr. Sci. 659 (2022) 120802, https://doi.org/10.1016/j.memsci.2022.120802.
[28] S. Zhang, R. Zhang, R. Li, Z. Zhang, Y. Li, H. Deng, J. Zhao, T. Gu, M. Long, X. Wang, S. Zhang, Z. Jiang, Guanidyl-incorporated nanofiltration membranes toward superior Li+/Mg2+ selectivity under weakly alkaline environment, J. Membr. Sci. 663 (2022) 121063, https://doi.org/10.1016/j.memsci.2022.121063.
[29] X. Xu, G. Hua, Y. Chen, Y. Zhang, Z. Zhang, W. Yang, F. Liu, A. Li, Dually charged polyamide nanofiltration membrane incorporated UiO-66-(NH2)2: Synergistic rejection of divalent cations and anions, Sep. Purif. Technol. 311 (2023) 123223, https://doi.org/10.1016/j.seppur.2023.123223.
[30] P. Giannozzi, S. Baroni, N. Bonini, M. Calandra, R. Car, C. Cavazzoni, D. Ceresoli, G.L. Chiarotti, M. Cococcioni, I. Dabo, A. Dal Corso, S. de Gironcoli, S. Fabris, G. Fratesi, R. Gebauer, U. Gerstmann, C. Gougoussis, A. Kokalj, M. Lazzeri, L. Martin-Samos, N. Marzari, F. Mauri, R. Mazzarello, S. Paolini, A. Pasquarello, L. Paulatto, C. Sbraccia, S. Scandolo, G. Sclauzero, A.P. Seitsonen, A. Smogunov, P. Umari, R.M. Wentzcovitch, QUANTUM ESPRESSO: a modular and open-source software project for quantum simulations of materials, J. Phys. Condens. Matter. 21 (39) (2009) 395502, https://doi.org/10.1088/0953-8984/21/39/395502.
[31] F. Soyekwo, H. Wen, D. Liao, C. Liu, Fouling-resistant ionic graft-polyamide nanofiltration membrane with improved permeance for lithium separation from $MgCl_2$/LiCl mixtures, J. Membr. Sci. 659 (2022) 120773, https://doi.org/10.1016/j.memsci.2022.120773.
[32] A.D. Allen, C.V. Senoff, INFRARED Spectra of tris-ethylenediamine complexes of ruthenium (II), Can. J. Chem. 43 (4) (1965) 888–895, https://doi.org/10.1139/v65-115.
[33] J. Zhao, X. You, G. Wang, J. Yuan, Y. Li, C. Yang, S. Zhang, X. Wang, R. Zhang, H. Wu, Z. Jiang, Mix-charged polyamide membranes via molecular hybridization for selective ionic nanofiltration, J. Membr. Sci. 644 (2022) 120051, https://doi.org/10.1016/j.memsci.2021.120051.